Highlights

Strain rate, temperature and deformation state effect on Ecoflex 00-50 silicone mechanical behaviour

Jacopo Lavazza, Marco Contino, Claudia Marano

- Extensive thermo-mechanical characterization of Ecoflex 00-50 silicone elastomer.
- Identification of a strain threshold for strain rate-independent mechanical response.
- Dependency of the strain rate-independent region extension on the deformation state.
- Negligible energy dissipation in the strain rate-independent region.
- Evaluation of strain rate and temperature effect on ultimate properties.

Strain rate, temperature and deformation state effect on Ecoflex 00-50 silicone mechanical behaviour

Jacopo Lavazza[a,1], Marco Contino[a], Claudia Marano[a]

[a]*Dipartimento di Chimica, Materiali e Ingegneria Chimica "G. Natta", Politecnico di Milano, Piazza Leonardo da Vinci 32, Milano, 20133, Italy*

Abstract

Silicone elastomers have attracted considerable attention due to their wide range of biomedical engineering and soft robotics applications. In this work, an extensive thermo-mechanical characterization of Ecoflex Shore hardness 00-50, a commercially available silicone elastomer, has been carried out to compensate for the lack of relevant literature. The mechanical behaviour of the material has been characterized by performing monotonic and cyclic loading tests. These tests were performed in different deformation states, i.e. uniaxial tension, pure shear and biaxial tension, at different strain rates and temperatures. Experimental findings allowed to highlight a time-dependent response of the material and to quantify the contribution of dissipative deformation phenomena to the overall strain energy. Uniaxial tensile tests performed at different temperatures (between -40°C and 140°C) showed that the material mechanical behaviour is sensitive to temperature in this range: a decrease of ultimate stress and strain has been observed with increasing temperature. Finally, the data obtained from the latter tests has been used to define a failure envelope, applied for the first time to Ecoflex silicones, and valuable to describe the material ultimate stress and strain at any temperature and strain rate.

Keywords: Ecoflex silicone elastomer, Thermo-mechanical characterization,

Email addresses: jacopo.lavazza@bristol.ac.uk (Jacopo Lavazza), marco.contino@polimi.it (Marco Contino), claudia.marano@polimi.it (Claudia Marano)

[1]Present affiliation: Bristol Composites Institute, Department of Aerospace Engineering, School of Civil, Aerospace, and Mechanical Engineering, University of Bristol, Queen's Building, University Walk, Bristol, BS8 1TR, UK

Deformation states, Dissipative behaviour

1. Introduction

Silicone elastomers have seen increasing interest in recent times because of their unique set of mechanical and physical properties, such as extremely low glass transition temperature (usually below -120°C), good thermal stability (in the temperature range from -50°C to 250°C), high hydrophobicity, chemical resistance and biocompatibility. Furthermore, silicones are typically characterized by large stretchability and low stiffness, closely matching those of compliant biological tissues [1, 2, 3]. This set of properties led to a variety of applications such as tubes, pumps and catheters in biomedical engineering [4], actuators and sensors in soft robotics and flexible electronics [5], as gaskets, diaphragms and sealants in the aerospace and automotive industries [6]. Silicones also find applications in the mechanobiology field as substrates [7].

Ecoflex™ (Smooth-On inc., USA) elastomers are commercially available silicones characterized by different Shore hardness ranging from Shore 00-10 to Shore 00-65; they are two-component platinum-catalyzed silicones, cured at room temperature in a relatively short time, from a few minutes to a couple of hours. Even if no information is provided by the producer on the chemical structure or the filler nature and content of the material, previous studies suggest they may be polydimethylsiloxane (PDMS) based elastomers, filled with silica to some extent [6, 8]. Due to their low viscosity, high biocompatibility and high stretchability, Ecoflex silicones are ideal candidates for applications in flexible sensors and biomedical actuation systems. For example, in [9, 10], super-stretchable, skin-mountable, and ultra-soft strain sensors based on Ecoflex-carbon nanotube nanocomposite thin films were developed. In [11], a method is proposed to manufacture bio-inspired Ecoflex/hydrogel hybrids with tough interfaces and functional microstructures. In [12], a strategy is proposed for printing conductors based on Ag ink onto Ecfolex/hydrogel stretchable substrates using a water-soluble tape. In [13], soft pneumatic actuators based on Ecoflex/paper composites were fabricated and tested. In [14], compression tests were performed on Ecoflex Shore 00-10 and Shore 00-30 to mimic the stress distribution in deep tissue injured muscles, and a preliminary patient simulator prototype was developed.

Finally, piezoelectric nanogenerators based on $BaTiO_3$/Ecoflex and carbon nanotubes (MWCNT)/Ecoflex composites for self-powered human motion and pressure monitoring were manufactured [15], and [16, 17], respectively.

Within this series of silicone rubbers, the mechanical behaviour of Ecoflex Shore 00-30 has been deeply studied and reported in literature. In [3], an extensive mechanical investigation was carried out through cyclic loading-unloading tests and single-step relaxation tests. The material resulted to be highly hysteretic, characterized by significant strain-induced stress softening (or Mullins effect, as originally proposed in [18]) during loading, as well as by a time-dependent behaviour, as clearly shown in stress relaxation tests. Furthermore, the study highlights that the material hysteretic behaviour is significantly reduced if the material is pre-stretched or undergoes a preliminary relaxation test before a tensile test is performed. It is suggested that this may be caused by material structural changes occurring when the material is deformed. It was observed that no residual strain is present after the unloading of the material, in contrast with what is reported in [8], where a significant residual set was observed for both Ecoflex Shore 00-30 and 00-50. As reported in [3], a very limited strain rate and temperature dependence of the mechanical response were observed for Ecoflex Shore 00-30.

In [19], tests similar to the previously described ones were performed on Ecoflex Shore 00-10, 00-20 and 00-50: it was found that all the considered Ecoflex grades have similar behaviour concerning time and temperature dependence, and that material stiffness, hysteretic behaviour, the range of time over which stress-relaxation phenomena occur, and strain-induced or relaxation induced softening, increase with the increase of Shore hardness. These results, although insightful of the material mechanical behaviour, are limited to the uniaxial tension deformation state; in order to completely describe the material response, other deformation states more resembling real application conditions should be tested; some preliminary results for pure shear and equibiaxial deformation states are reported in [20], where larger apparent stress softening is observed for pure shear and equibiaxial deformation modes with respect to uniaxial tension; furthermore, residual deformation after unloading, which was not observed in uniaxial tensile tests in [3], is noted in the other deformation states.

To the best of the authors' knowledge, the ultimate tensile stress (σ_U) and

strain (ϵ_U) of Ecoflex elastomers, and their dependence on time and temperature, have not been investigated in literature. Because of the large variability of these two quantities, depending on testing conditions, it has been difficult to relate unambiguously ultimate properties to the molecular structure of an elastomer: a possible approach, based on the concept of "failure envelope", has been proposed in [21, 22] for unfilled elastomers; from creep tests, it was observed that it is possible to obtain a curve, defined by the failure points of the material, which is independent of time and temperature. This envelope, which is unique for every material, is indicative of the topological characteristics of a specific polymeric network. This approach was further investigated in [23]: considering a sample subjected to a constant load test (creep test), the material will undergo a progressively increasing macroscopic elongation while, at a microscopic level, small tears will form and start to grow. In [24], it was proposed that the time taken for the material at the tear tip to rupture is determined by the rate of retraction of the broken filament and the creep response of the subsequent filament to the load to which it is subjected. Therefore, the tear propagation rate that controls the time to failure t_U is determined by the creep response (i.e. the creep compliance) of the elastomer. In the same papers, it was observed that these considerations could be extended to tensile tests, too, obtaining a singular failure envelope: based on these considerations, the ultimate stress and strain can be computed from the creep compliance of the material in any loading condition.

Despite the presence of comprehensive studies on the mechanical behaviour of Ecoflex Shore 00-30 in literature, Ecoflex polymers of different Shore hardness have been studied in a much more limited way; furthermore, in most applications, the deformation state to which components are subjected is more complex than uniaxial extension. Therefore, this experimental work aims at providing an in-depth study on Ecoflex Shore 00-50 mechanical behaviour, starting from already available observations present in literature and including missing information regarding the effect of different modes of deformation and temperature on the material response, focusing in particular on ultimate tensile properties.

The manuscript is structured as follows: in Section 2, the details about the adopted material and specimen preparation are presented, alongside the different testing setups and the testing campaign performed. Furthermore, details about the calculation of the energy density associated with cyclic ten-

sile tests are reported. Section 3 presents the theoretical details concerning the comparison of the material mechanical response in different deformation states, applied in the following section to compare and discuss experimental data. In Section 4, the experimental details are presented and discussed, considering monotonic and cyclic tensile tests, in addition to the effects of temperature on Ecoflex 00-50 ultimate properties. Finally, the main findings and observations are summarized in Section 5.

2. Experimental details

2.1. Material preparation and adopted specimens

Ecoflex Shore 00-50 was provided in two liquid components, mixed in a 1:1 weight ratio, and thoroughly mixed for 5 minutes with a mechanical mixer, working at 600 rpm. Afterwards, the mixture was cast in the bottom half of a mould which was placed for 10 minutes in a vacuum oven at 23°C and -0.9 Pa to remove entrapped air and minimize bubble presence in the material. Then, within the material pot life of 18 minutes, the mould was closed with its upper half, and the material was left to polymerize and crosslink for 3 hours at 23°C. Different moulds were used to obtain specimens of different geometries.

The material was tested in three different deformation states, namely uniaxial tension (UT), pure shear (PS) and equibiaxial tension (ET). The UT state is such that the elementary volume is deformed along one principal direction ($\lambda_1 = \lambda$) and left free to contract in the other two; calling λ_2 the in-plane orthogonal direction and λ_3 the direction perpendicular to the plane, and assuming constant volume deformations (i.e. $\lambda_1\lambda_2\lambda_3 = 1$), one obtains that $\lambda_2 = \lambda_3 = 1/\sqrt{\lambda}$. In the PS state, the contraction in the in-plane orthogonal direction is prevented ($\lambda_2 = 1$), and so $\lambda_3 = 1/\lambda$. In the case of ET state, the in-plane principal stretches are equal ($\lambda_1 = \lambda_2 = \lambda$), and therefore $\lambda_3 = 1/\lambda^2$.

In order to achieve the different deformation states, different specimen geometries were adopted during testing, which are illustrated in Figure 1: the short strip-shaped specimens (Figure 1b) were used in place of the dumbbell specimens (Figure 1a) to test the material at temperatures different than 23°C (see Section 4.3): these tests were carried out in an environmental chamber, in which the crosshead displacement is limited to about 200 mm.

For PS, ET and strip-shaped specimens, a thicker border is needed to fix the specimens in the adopted clamping systems.

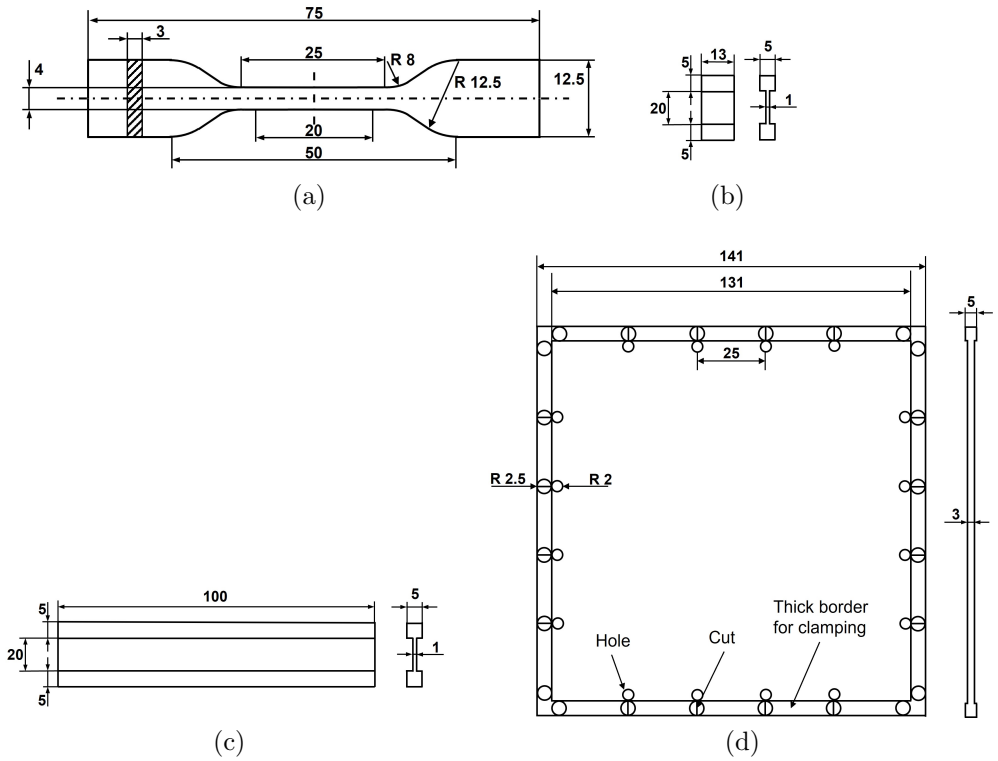

Figure 1: Geometry and dimensions (in mm) of the specimens used for tests in uniaxial tension (1a and 1b), pure shear (1d) and equibiaxial tension (1c) deformation states.

2.2. Experimental set-up

Uniaxial tensile tests and pure shear tests were performed on an Instron 5967 screw-driven dynamometer equipped with a 2 kN load cell. UT tests were video recorded to evaluate the variation of the distance ΔL between two black marks drawn on each specimen at an initial distance $L_0 = 20$ mm; the strain was evaluated accordingly. In the case of PS tests, the strain along the stretching direction was evaluated as the ratio between the crosshead displacement and the specimen gauge length after verification of negligible testing machine compliance.

Equibiaxial tension tests were performed on the custom-built biaxial dynamometer shown in Figure 2. The machine is equipped with two 25 kN

load cells along one of the loading directions and two 50 kN load cells in the other direction. Five clamps for each side are mounted on rails and free to slide during the test to adapt to the deformation in different directions. Further details on the testing setup can be found in [25]. In this case, strains were determined through Digital Image Correlation (DIC) analysis by applying a speckle pattern to the specimen surface. Stress and strain were computed by averaging the values obtained in the two orthogonal loading directions.

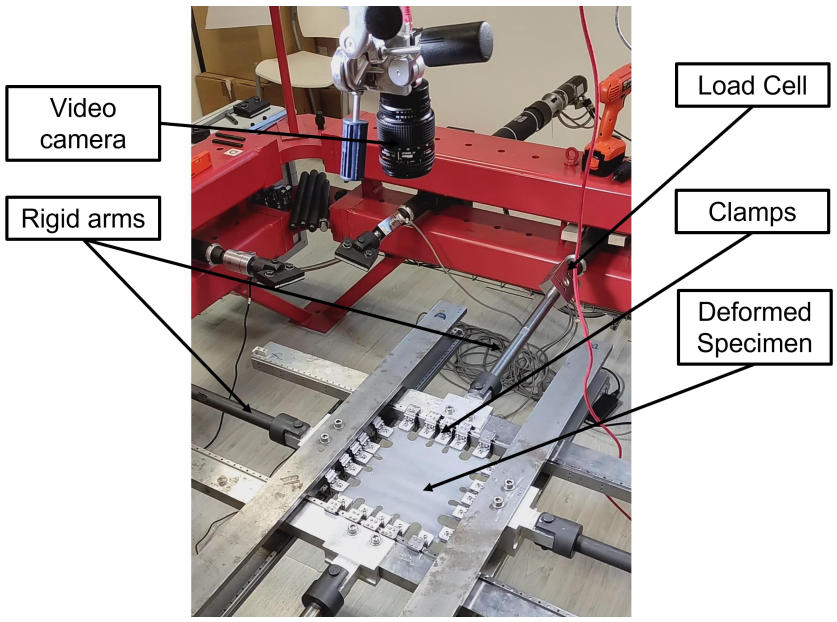

Figure 2: The custom-built biaxial test setup with the clamping system, designed in [25], consisting of four rigid arms, equipped with two 25 kN and two 50 kN load cells. The specimen is mounted in a custom-built clamping system, free to slide during testing. The test is video recorded through a video camera mounted parallel to the specimen surface.

Tests at different temperatures (ranging between -40°C and 140°C, see Section 2.3) were performed on an Instron 5967 dynamometer equipped with a 2 kN load cell and an environmental chamber, using a liquid CO_2 based cooling system to reach temperatures lower than 23°C. Strains were determined as the ratio between the crosshead displacement and the specimen gauge length since the testing machine compliance, as already reported, was negligible.

In all video-recorded tests, a 10 MPixel uEye UI 5490 SE camera was used, with a framerate between 1 and 20 fps (defined to obtain at least 1000 frames for each test, depending on their duration).

2.3. Experimental tests

Monotonic tensile tests at room temperature and in different deformation states were performed at different strain rates until specimen failure. Several specimens were tested in each condition in order to quantify the response variability:

- nine UT specimens were tested at three different nominal strain rates ($0.1\ s^{-1}$, $0.01\ s^{-1}$ and $0.005\ s^{-1}$);
- five PS specimens were tested at two different nominal strain rates ($0.1\ s^{-1}$ and $0.01\ s^{-1}$);
- four ET specimens were tested at $\dot{\epsilon} = 0.05\ s^{-1}$ and one at $\dot{\epsilon} = 0.001\ s^{-1}$.

Cyclic tensile tests at room temperature and in different deformation states were performed at different nominal strain rates and up to different values of maximum nominal strain, ranging between $\epsilon = 1$ and $\epsilon = 5$:

- four UT specimens were tested for each value of maximum nominal strain (tested at both $0.1\ s^{-1}$ and $0.01\ s^{-1}$);
- four PS specimens were tested for each value of maximum nominal strain (tested at both $0.1\ s^{-1}$ and $0.01\ s^{-1}$);
- one ET specimen was tested up to $\epsilon = 1$ (tested at $0.05\ s^{-1}$).

The effect of temperature on the material mechanical response was investigated by performing tests at -40°C, -20°C, 0°C, 23°C, 60°C, 80°C, 100°C and 140°C: this temperature range was chosen in order to have a direct comparison with already available data, present in [3, 19] for Ecoflex 00-30. The upper limit was fixed to avoid material degradation during testing. For each temperature, four strip specimens (see Figure 1b) were tested at $\dot{\epsilon} = 0.1\ s^{-1}$ after conditioning for 15 minutes. Furthermore, tests at different nominal strain rates ($0.1\ s^{-1}$, $0.01\ s^{-1}$ and $0.001\ s^{-1}$) were performed at 23°C, 60°C and 100°C.

2.4. Identification of energy density from cyclic tensile tests

In Section 4.2, the energy density associated with each loading-unloading cycle was determined from experimental data obtained during cyclic tensile tests. The dissipated energy density (w_d) was calculated by integration of the area between the loading and unloading curves, whereas the stored energy density (w_s) was calculated by integration of the area beneath the unloading path (as shown in Figure 3).

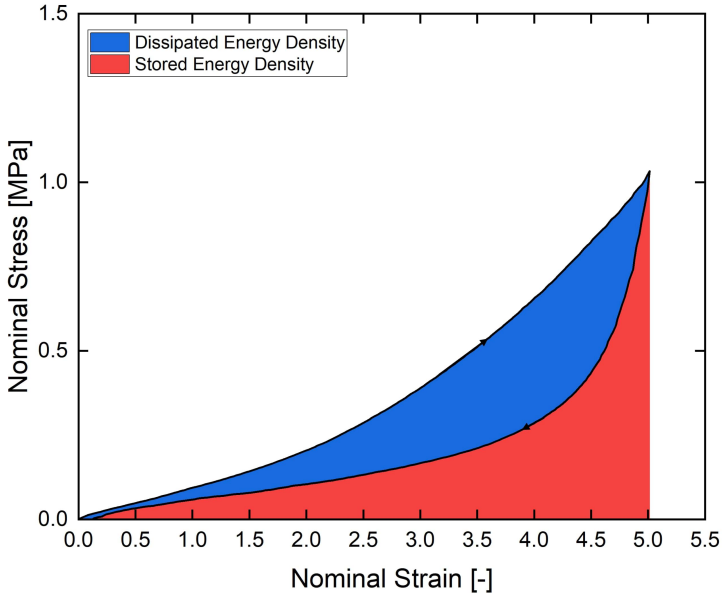

Figure 3: Definition of dissipated (blue) and stored (red) energy densities from loading-unloading test.

The sum of the two contributions is the total energy density (w_{tot}) associated with the loading-unloading cycle:

$$w_{tot} = w_d + w_s = \left(\int_l \sigma d\epsilon - \int_{ul} \sigma d\epsilon \right) + \int_{ul} \sigma d\epsilon = \int_l \sigma d\epsilon \qquad (1)$$

where the subscripts l and ul identify the loading and unloading paths, respectively.

3. Comparison of different deformation states

To summarize the results obtained in Section 4.1 in the different deformation states, an alternative way of representing stress-strain curves is presented to

clearly compare experimental data, following the derivation reported in [26]. Assuming a Neo-Hookean behaviour, the strain energy function is defined as [27]:

$$W = \frac{G}{2}(I_1 - 3) \tag{2}$$

where G is the shear modulus of the material and I_1 is the first stretch invariant, which is equal to $\lambda_1^2+\lambda_2^2+\lambda_3^2$, being λ_i the principal stretches ($\lambda_i = \epsilon_i+1$, where ϵ_i are the principal nominal strains). For an ideal incompressible elastomer $\lambda_1\lambda_2\lambda_3 = 1$ and $\lambda_3 = 1/(\lambda_1\lambda_2)$, therefore Equation (2) can be written explicitly as:

$$W = \frac{G}{2}\left(\lambda_1^2 + \lambda_2^2 + \frac{1}{\lambda_1^2\lambda_2^2} - 3\right) \tag{3}$$

The nominal stress-stretch relationship can be obtained by derivation of Equation (3), as:

$$\sigma_1 = \left(\frac{\partial W}{\partial \lambda_1}\right) = G\left(\lambda_1 - \frac{1}{\lambda_1^3\lambda_2^2}\right) \tag{4}$$

The first true principal stress is defined as $\sigma_{t,1} = \lambda_1\sigma_1$ which, combined with the incompressibility relation, leads to:

$$\sigma_{t,1} = \lambda_1\sigma_1 = G(\lambda_1^2 - \lambda_3^2) \tag{5}$$

A similar expression is obtained for $\sigma_{t,2}$ and, in the case of plane stress ($\sigma_{t,3} = 0$), the general true stress state is defined as:

$$\begin{cases} \sigma_{t,1} = G(\lambda_1^2 - \lambda_3^2) \\ \sigma_{t,2} = G(\lambda_2^2 - \lambda_3^2) \\ \sigma_{t,3} = 0 \end{cases} \tag{6}$$

The difference between the first and second true principal stresses will always be proportional to the difference between the first and second principal stretches squared:

$$\sigma_{t,1} - \sigma_{t,2} = G(\lambda_1^2 - \lambda_2^2) \tag{7}$$

In particular, for UT, PS, and ET deformation states, the expression is simplified to:

$$\begin{cases} \sigma_{t,1} - \sigma_{t,2} = G\left(\lambda_1^2 - \dfrac{1}{\lambda_1}\right) & for\ \boldsymbol{UT} \\ \sigma_{t,1} - \sigma_{t,2} = G\left(\lambda_1^2 - 1\right) & for\ \boldsymbol{PS} \\ \sigma_{t,1} - \sigma_{t,2} = G\left(\lambda_1^2 - \dfrac{1}{\lambda_1^4}\right) & for\ \boldsymbol{ET} \end{cases} \tag{8}$$

Notice that, according to the definition reported in [26], for the ET state $\lambda_1 = \lambda_3 = \lambda$, and therefore $\lambda_2 = 1/\lambda^2$. Equation (8) can be expressed in terms of nominal stress and stretch as follows:

$$\begin{cases} \sigma\lambda = G\left(\lambda^2 - \dfrac{1}{\lambda}\right) & for\ \boldsymbol{UT} \\ \sigma\lambda\left(1 - \dfrac{1}{\lambda^2+1}\right) = G\left(\lambda^2 - 1\right) & for\ \boldsymbol{PS} \\ \sigma\lambda = G\left(\lambda^2 - \dfrac{1}{\lambda^4}\right) & for\ \boldsymbol{ET} \end{cases} \tag{9}$$

Finally, the value of shear modulus can be obtained by fitting the region of the stress-strain curves, which showed an overall decreasing slope (corresponding to $\epsilon \leq 1$ for UT and PS and to $\epsilon \leq 0.3$ for ET) through the use of the Neo-Hookean model, as already proposed in [19]. The Neo-Hooke model expression is obtained by rearranging Equation (9) as:

$$\sigma = \begin{cases} G\left(\lambda - \dfrac{1}{\lambda^2}\right) & for\ \boldsymbol{UT} \\ G\left(\lambda - \dfrac{1}{\lambda^3}\right) & for\ \boldsymbol{PS} \\ G\left(\lambda - \dfrac{1}{\lambda^5}\right) & for\ \boldsymbol{ET} \end{cases} \tag{10}$$

4. Results and discussion

4.1. Monotonic tensile tests

Ecoflex 00-50 uniaxial tension specimens (see Figure 1a) were tested at different nominal strain rates, namely $\dot{\epsilon} = 0.1\ s^{-1}$, $\dot{\epsilon} = 0.01\ s^{-1}$ and $\dot{\epsilon} = 0.005\ s^{-1}$,

in order to investigate the time-dependency of the material mechanical response. The nominal stress-strain curves for uniaxial tensile tests performed at the different strain rates are reported in Figure 4.

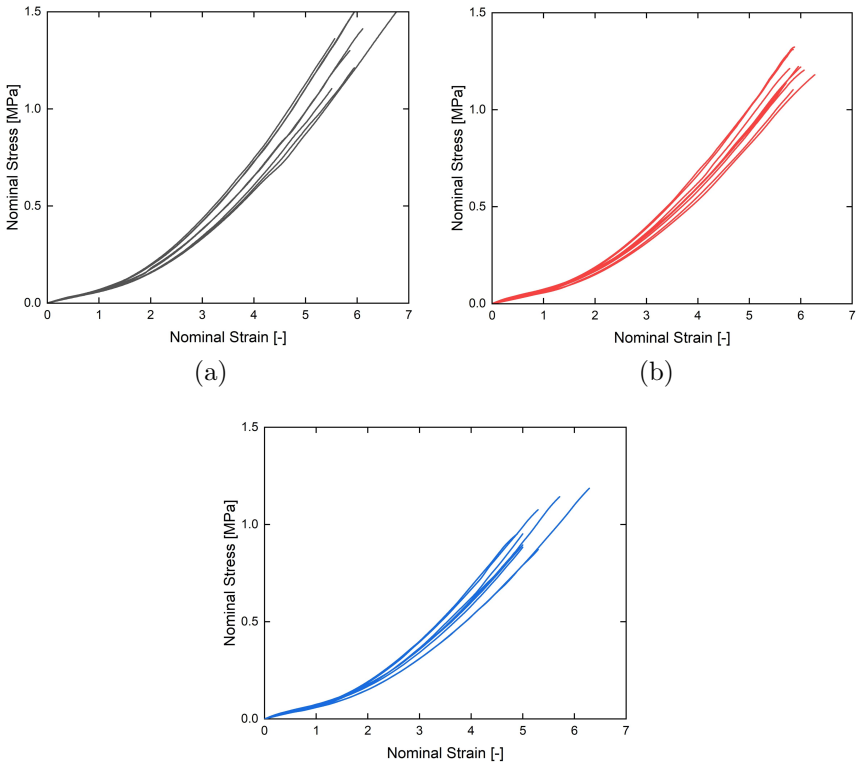

Figure 4: Ecoflex 00-50 nominal stress-strain curves for uniaxial tension tests, performed at 4a) $\dot{\epsilon} = 0.1\ s^{-1}$, 4b) $\dot{\epsilon} = 0.01\ s^{-1}$ and 4c) $\dot{\epsilon} = 0.005\ s^{-1}$. All tests performed at T = 23°C.

Some degree of variability is observed among curves obtained from tests at the same strain rate, which could be attributed to experimental errors in the specimen preparation process (e.g. micro-bubbles formed during casting, defects at the specimen edge from die-cutting etc.) or to some structural inhomogeneity of the material. To better compare the material behaviour at different strain rates, the highest and lowest experimental stress-strain curves with variability intervals (the area between the two curves) for each test are reported in Figure 5; in this representation, ultimate stresses and strains are

not considered meaningful.

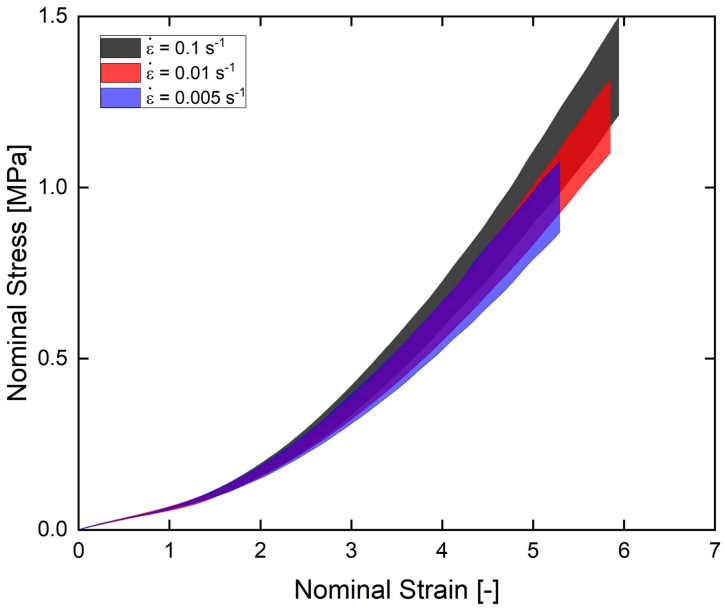

Figure 5: Ecoflex 00-50 nominal stress-strain curves for uniaxial tension tests, performed at T = 23°C and $\dot{\epsilon} = 0.1\ s^{-1}$ (black curve), $\dot{\epsilon} = 0.01\ s^{-1}$ (red curve) and $\dot{\epsilon} = 0.005\ s^{-1}$ (blue curve).

No significant difference is observed between the curves relevant to tests performed at $\dot{\epsilon} = 0.01\ s^{-1}$ and $\dot{\epsilon} = 0.005\ s^{-1}$. It is possible to notice that all the curves superimpose for strains lower than $\epsilon \approx 2$, suggesting a strain rate independence of the mechanical behaviour in this range. At larger strains, for a given deformation, the stress increases, increasing the deformation rate, especially for the curves at $\dot{\epsilon} = 0.1\ s^{-1}$. The averaged values, with relevant standard deviation, of tensile modulus (E) evaluated at $\epsilon = 0.1$, and ultimate strain (ϵ_U) and stress (σ_U) for each strain rate are reported in Table 1: an increase of both ultimate strain and ultimate stress is observed with increasing strain rate, mainly for stress values.

Strain Rate, $[s^{-1}]$	$E(\epsilon = 0.1)$, **[MPa]**	ϵ_U, **[-]**	σ_U, **[MPa]**
0.1	0.08 ± 0.01	5.87 ± 0.49	1.34 ± 0.16
0.01	0.08 ± 0.02	5.94 ± 0.18	1.22 ± 0.06
0.005	0.08 ± 0.01	5.29 ± 0.45	0.99 ± 0.12

Table 1: Averaged values (with relevant standard deviation) of tensile modulus (evaluated at $\epsilon = 0.1$), ultimate strain and ultimate stress for the different strain rates considered in uniaxial tension tests.

The stress and strain at failure obtained for $\dot{\epsilon} = 0.1\ s^{-1}$ are comparable with those reported in [19] of $\epsilon_U = 6.5$ and $\sigma_U = 1.6$ MPa, although being slightly lower. Furthermore, as expected, practically no variation of tensile modulus is observed with varying strain rate.

The nominal stress-strain curves for monotonic tensile tests performed on PS specimens (see Figure 1c) at different strain rates, namely $\dot{\epsilon} = 0.1\ s^{-1}$ and $\dot{\epsilon} = 0.01\ s^{-1}$, are reported in Figure 6. It should be noted that, for all specimens, failure occurred near the thick clamped edges, most likely due to stress intensification, so stress and strain values at break have not been considered in this study.

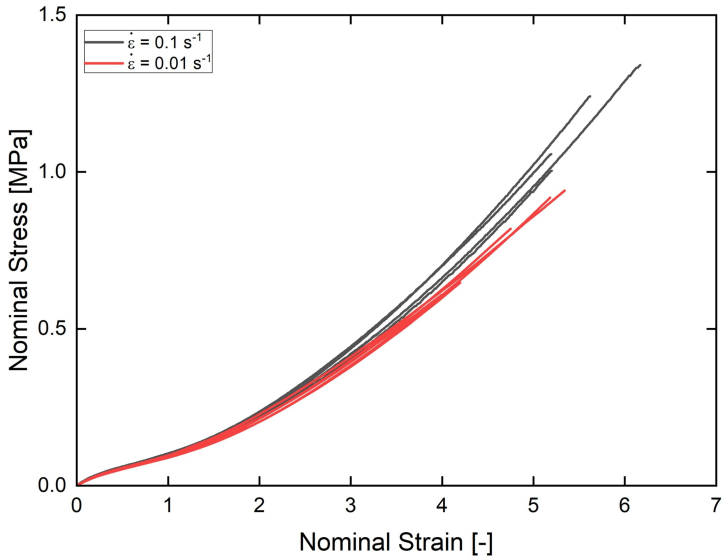

Figure 6: Ecoflex 00-50 nominal stress-strain curves for pure shear tests, performed at $\dot{\epsilon} = 0.1\ s^{-1}$ (black curves) and $\dot{\epsilon} = 0.01\ s^{-1}$ (red curves). All tests performed at T = 23°C.

The curves corresponding to the PS specimen tested at $\dot{\epsilon} = 0.01\ s^{-1}$ show a very limited variability compared to UT curves. Similarly to UT tests, the portion of the curves up to $\epsilon \approx 2$ is unaffected by strain rate variations. In contrast, an increase in stress with increasing strain rate is clearly noticeable at higher strains.

The nominal stress-strain curves of different equibiaxial tension tests, performed at $\dot{\epsilon} = 0.05\ s^{-1}$ and $\dot{\epsilon} = 0.001\ s^{-1}$, are reported in Figure 7. A single curve is reported for each strain rate because of the limited tests performed.

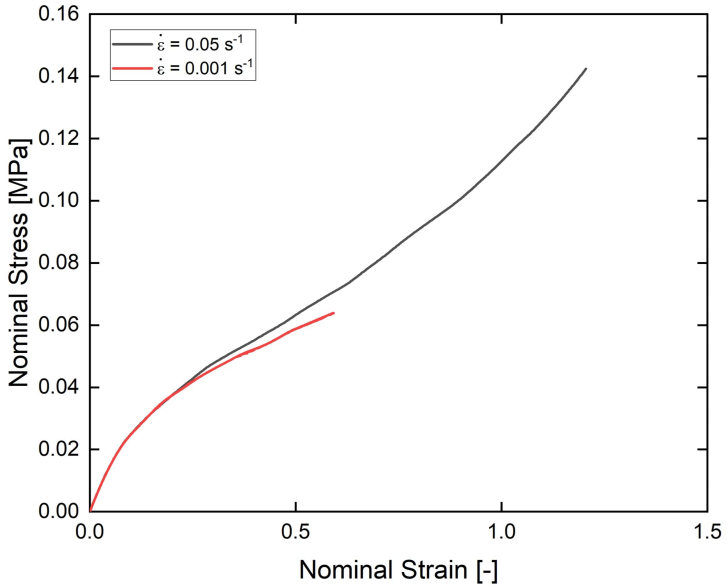

Figure 7: Ecoflex 00-50 nominal stress-strain curves for equibiaxial tension tests, performed at $\dot{\epsilon} = 0.05\ s^{-1}$ (black curve) and $\dot{\epsilon} = 0.001\ s^{-1}$ (red curve). All tests performed at T = 23°C.

It is noticeable how failure occurs at ultimate strain much lower than those observed for UT and PS tests, despite always starting from the holes at the border of the specimen (see Figure 1d), due to stress intensification. A negligible strain rate effect is observed for $\epsilon < 0.3$ although, given the limited experimental data available, this effect should be further investigated with more tests.

In order to compare the results obtained in different deformation states, the

derivation presented in Section 3 was applied to the experimental data obtained during the monotonic tests. The shear modulus G was determined by simultaneously fitting Equation (10) to experimental data in the strain rate independent region ($\epsilon \approx 1$ for UT and PS, and $\epsilon \approx 0.3$ for ET) obtained in the different deformation states, through the use of least square curve-fitting approach (*lsqcurvefit*) built-in the commercially available software MATLAB. The obtained value of shear modulus is $G = 0.044$ MPa: no data is available in literature regarding measured values of shear modulus for Ecoflex 00-50, but the value is comparable to that reported in [19] of $G = 0.039$ MPa, determined by a Shore hardness amplification factor multiplied by the G value estimated from UT data for the lower hardness Ecoflex 00-10. The comparison between experimental data and the Neo-Hookean model is reported in Figure 8.

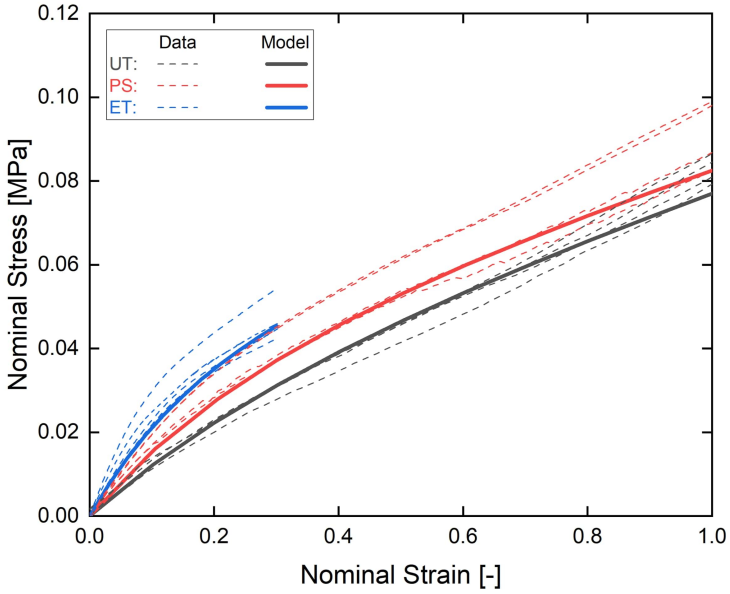

Figure 8: Comparison of experimental data (dashed lines) and Neo-Hookean model with $G = 0.044$ MPa (see Equation (10), continuous lines). Experimental nominal stress-strain curves for uniaxial tension, pure shear and equibiaxial tension deformation states obtained at T = 23°C.

Despite the experimental data dispersion, it can be seen that the model properly describes the response of the material in all three deformation states. However, it slightly overestimates the response in UT and underestimates

the one in PS.

Since the value of G has been determined, it is possible to represent experimental data obtained in the different deformation states on a common $(\sigma_{t,1} - \sigma_{t,2})$ vs $(\lambda_1^2 - \lambda_2^2)$ plot (according to Equation (9)), as shown in Figure 9. The curves for PS and ET states correspond to a specimen tested at $\dot{\epsilon} = 0.05\ s^{-1}$, whereas the curve for the UT state corresponds to a specimen tested at $\dot{\epsilon} = 0.01\ s^{-1}$, since no strain rate influence is observed in this range. For the theoretical trend, the value of $G = 0.044$ MPa was used.

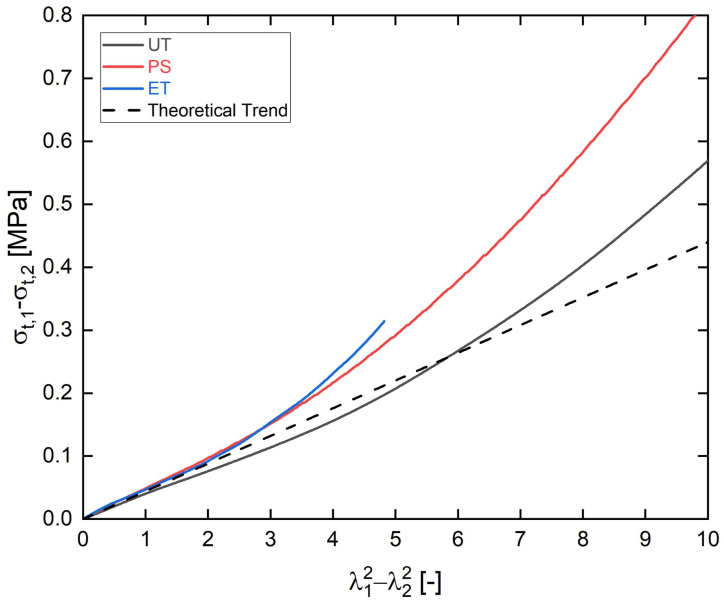

Figure 9: Difference of true principal stresses $(\sigma_{t,1} - \sigma_{t,2})$ vs Difference of true principal stretches $(\lambda_1^2 - \lambda_2^2)$ plot. Comparison between the experimental curves obtained in different deformation states at T = 23°C (see Equation (8), continuous lines) with the theoretical linear trend (see Equation (7), dashed line).

It can be seen how the three curves corresponding to the different deformation states converge, as expected, to the theoretical linear trend (Equation (7)) for $\lambda_1^2 - \lambda_2^2 \leq 1$. The PS and ET data agree with the theoretical trend up to larger strain values than UT. Furthermore, it can be seen that for both PS and ET states, the theoretical trend underestimates the real material response whereas, on the contrary, the UT response is overestimated for $1 \leq \lambda_1^2 - \lambda_2^2 \leq 6$. The deviation from linearity and the upward trend observed

for large strains are indicative of the limits of the Neo-Hookean description, which neglects finite chain extensibility and, therefore, the strain stiffening observed in Ecoflex 00-50 [26].

4.2. Cyclic tensile tests

The cyclic loading behaviour of Ecoflex 00-50 was investigated by performing multiple loading-unloading uniaxial tensile tests for different values of the applied strain. The nominal stress-strain curves corresponding to the first loading-unloading cycle, performed on five UT specimens stretched up to different nominal strains, are reported in Figure 10.

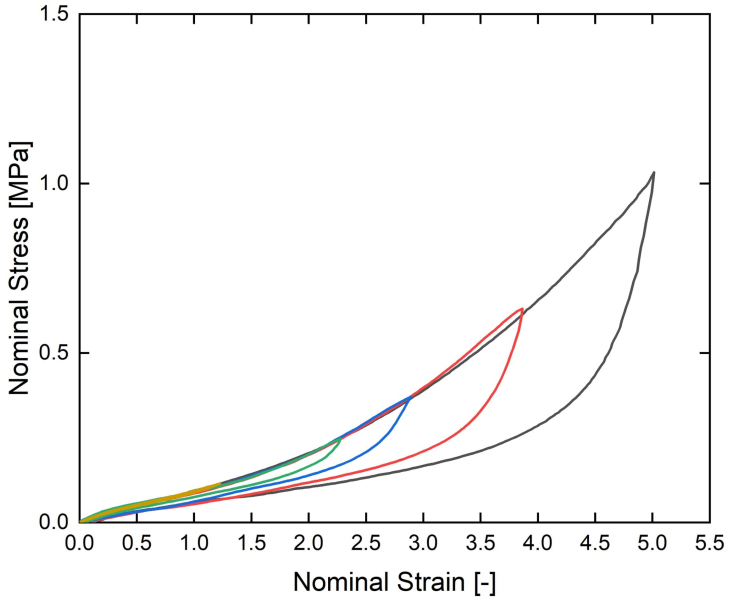

Figure 10: Ecoflex 00-50 nominal stress-strain plot of first loading-unloading cycle in uniaxial tension conditions. Tests performed on different specimens at $\dot{\epsilon} = 0.01\ s^{-1}$ and T = 23°C.

It can be seen how the loading and unloading paths of a cycle do not coincide, except for tests performed up to $\epsilon \approx 1.2$, suggesting a hysteretic (that is, dissipative) behaviour of the material. The dissipative behaviour was quantified through the calculation of the dissipated energy density associated with a loading-unloading cycle, as presented in Section 2.4. The dependence on the nominal strain of the total, dissipated and stored energy densities for the first

cycle, obtained from cyclic tests performed at $\dot{\epsilon} = 0.1\ s^{-1}$ and $\dot{\epsilon} = 0.01\ s^{-1}$, is reported in Figure 11.

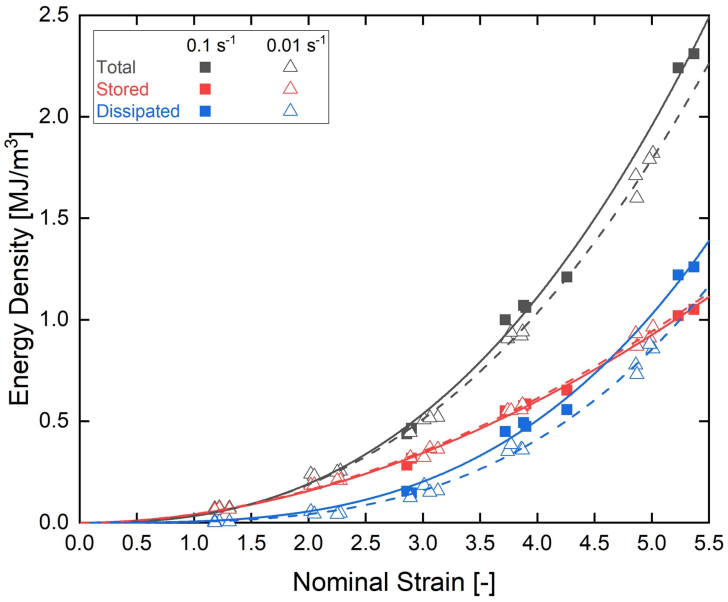

Figure 11: Strain dependence of total (black), dissipated (blue) and stored (red) energy densities relevant to the first cycle for uniaxial tension virgin specimens tested at $\dot{\epsilon} = 0.1\ s^{-1}$ (full squares) and $\dot{\epsilon} = 0.01\ s^{-1}$ (empty triangles). Fitting of data obtained from tests performed at $\dot{\epsilon} = 0.1\ s^{-1}$ (continuous lines) and $\dot{\epsilon} = 0.01\ s^{-1}$ (dashed lines). All tests performed at T = 23°C.

As expected, both energy density components increase with increasing applied strain. In particular, significant dissipation occurs for strains larger than $\epsilon \approx 2$. Furthermore, it can be seen how w_d remains almost half of w_s between $\epsilon = 2$ and $\epsilon = 4$, but for larger strain levels, the dissipated component becomes almost equal to the stored one. As reported in Section 4.1, an increase in strain rate leads to an increase of stress in the time-dependent region of the material response, and this effect is valid also during cyclic loading; therefore, tests at $0.1\ s^{-1}$ were performed only at strains larger than $\epsilon = 3$. An increase in total energy density is observed with increasing strain rate, which is associated with an increase in dissipated energy density; on the other hand, no net increase in stored energy density is associated with an increase in strain rate.

Residual strain is present at the end of unloading (even for tests performed up to $\epsilon \approx 1.2$, where negligible energy dissipation is observed), and it follows a quasi-linear trend with respect to the imposed maximum strain, as shown in Figure 12.

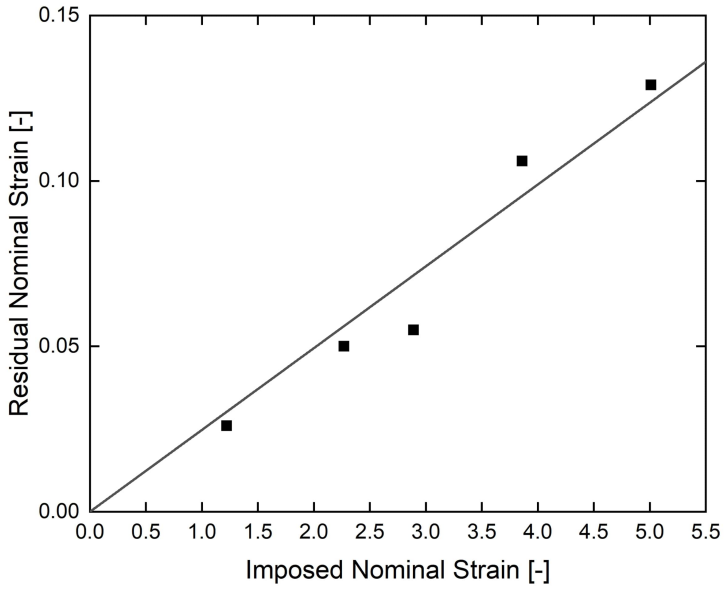

Figure 12: Residual strain at the end of the first loading-unloading cycle, for virgin uniaxial tension specimens tested up to different strains at $\dot{\epsilon} = 0.01\ s^{-1}$. All tests performed at T = 23°C.

In Figure 13 some of the curves for a 10 cycles cyclic loading test, performed on a single specimen stretched up to $\epsilon \approx 5$ at $\dot{\epsilon} = 0.01\ s^{-1}$, are reported.

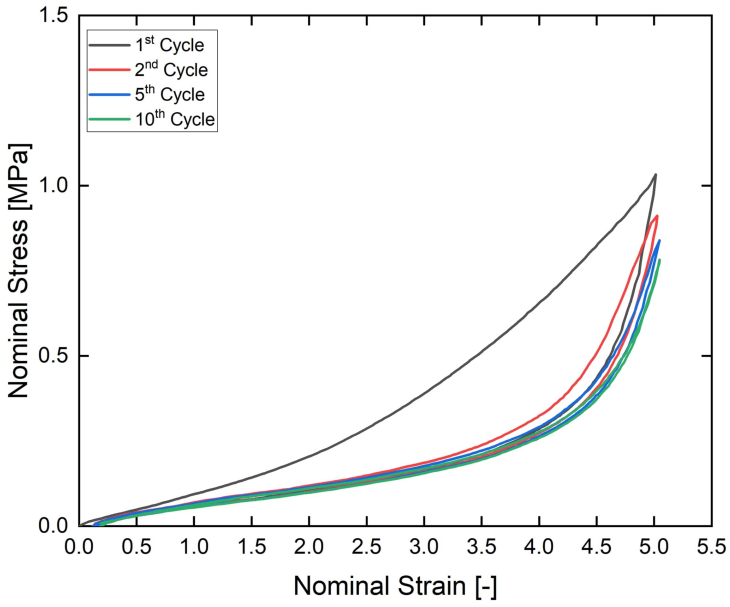

Figure 13: Ecoflex 00-50 nominal stress-strain plot of a multicycle uniaxial tension loading-unloading test. Test performed on a single specimen at $\dot{\epsilon} = 0.01\ s^{-1}$ and T = 23°C. The curves are relevant to the first, second, fifth and tenth loading-unloading cycles.

The hysteresis decreases with the number of cycles considered, as shown in Figure 14. It is evident that strain-induced stress softening (or Mullins effect) is present and mainly occurs during the first loading cycle. After the fifth cycle, the dissipated energy density becomes constant, and the maximum stress is reduced by less than 5% between two subsequent cycles (considered a negligible reduction), identifying the stabilized cyclic response of the material.

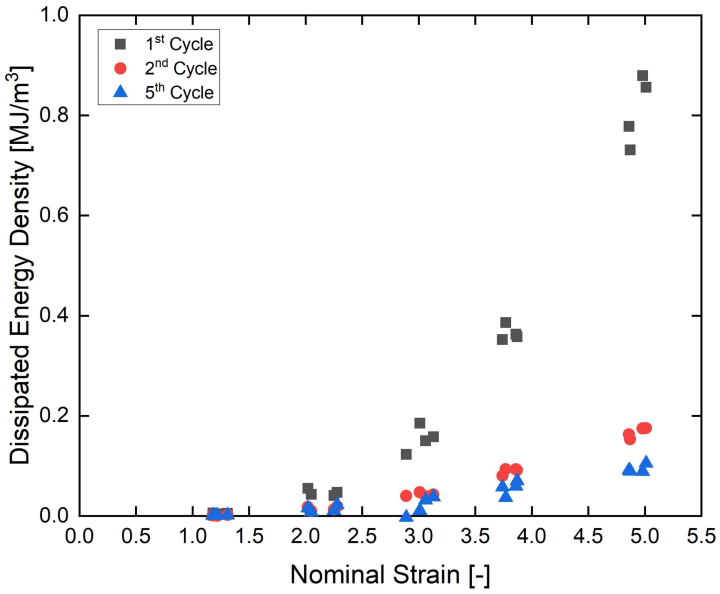

Figure 14: Dissipated energy density as a function of nominal strain. Data relevant to the first (black squares), second (red circles) and fifth (blue triangles) cycle. Data obtained from uniaxial tension cyclic tests performed up to different strains at $\dot{\epsilon} = 0.01\ s^{-1}$ and T = 23°C.

Up to $\epsilon \approx 2$ negligible hysteretic behaviour and softening are observed with an increasing number of cycles. On the contrary, for larger strains, an increase in stress softening and dissipation is associated with the number of cycles considered. These last observations are in agreement with the results reported in [3, 19], although no residual deformation was reported for UT tests.

Similar results were also obtained from the pure shear cyclic tests. The first cycle nominal stress-strain curves for several PS specimens subjected to cyclic loading at different strains are reported in Figure 15.

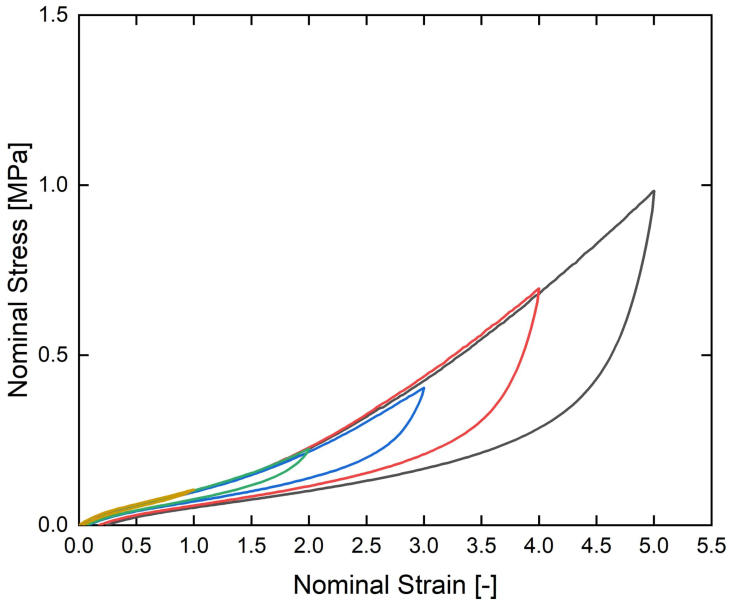

Figure 15: Ecoflex 00-50 nominal stress-strain plot of first loading-unloading cycle in pure shear conditions. Tests performed on different specimens at $\dot{\epsilon} = 0.1\ s^{-1}$ and T = 23°C.

For the cyclic tensile test in PS state, too, for strains up to $\epsilon = 1$, the hysteresis area is practically negligible. The total, stored and dissipated energy densities relevant to the first cycle are reported in Figure 16 as a function of the nominal strain, obtained from cyclic tests performed at $\dot{\epsilon} = 0.1\ s^{-1}$ and at $\dot{\epsilon} = 0.01\ s^{-1}$.

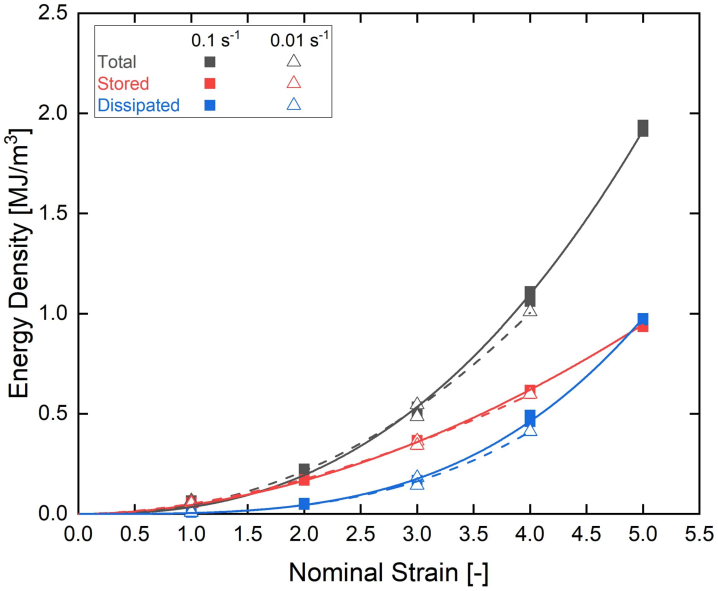

Figure 16: Strain dependence of total (black), dissipated (blue) and stored (red) energy densities relevant to the first cycle for pure shear virgin specimens tested at $\dot{\epsilon} = 0.1\ s^{-1}$ (full squares) and $\dot{\epsilon} = 0.01\ s^{-1}$ (empty triangles). Fitting of data obtained from tests performed at $\dot{\epsilon} = 0.1\ s^{-1}$ (continuous lines) and $\dot{\epsilon} = 0.01\ s^{-1}$ (dashed lines). All tests performed at T = 23°C.

The trends of both energy density components are very similar to those observed for UT cyclic tests, where the dissipated component is negligible for $\epsilon \leq 2$ and is approximately half the stored energy density for strains between $\epsilon = 2$ and $\epsilon = 4$. Furthermore, the strain rate has a very limited effect on the energy density components since a slight variation is observed only at $\epsilon = 4$. In contrast, for lower strain, the two components values are almost identical for the two strain rates considered. Results at larger strains may have helped confirm this strain rate effect but for specimens stretched up to $\epsilon = 5$ at $\dot{\epsilon} = 0.01\ s^{-1}$, premature failure occurred during the unloading of the first cycle.

Because of the limited extensibility of Ecoflex 00-50 in equibiaxial tension deformation state, cyclic tests were performed only up to $\epsilon \approx 1$ imposed maximum strain in both stretching directions. Only five cycles were performed during testing. The nominal stress-strain curves for an ET specimen subjected to cyclic loading at $\dot{\epsilon} = 0.05\ s^{-1}$ are reported in Figure 17.

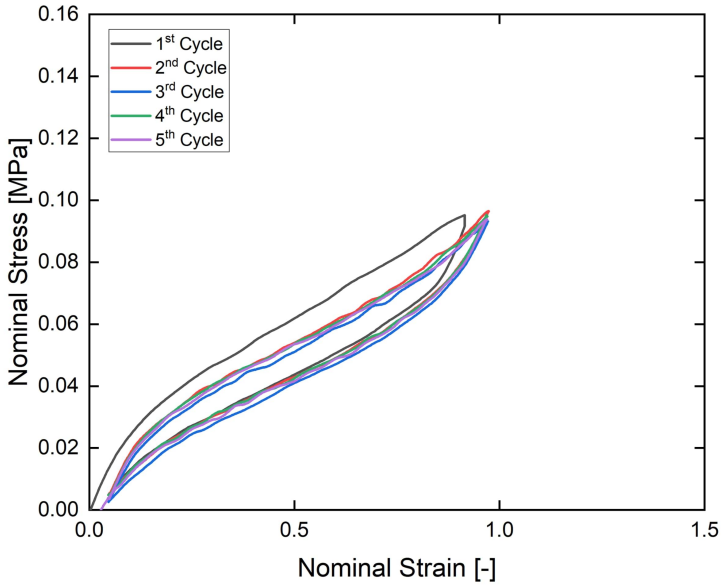

Figure 17: Ecoflex 00-50 nominal stress-strain plot of loading-unloading cycles of an equibiaxial tension cyclic test, performed up to $\epsilon \approx 1$ at $\dot{\epsilon} = 0.05\ s^{-1}$ and T = 23°C.

Differently to what was observed for the UT and PS cyclic tests up to $\epsilon \approx 1$, energy dissipation is not negligible in the cyclic ET test: this is in agreement with what is observed during ET monotonic tests, where the strain rate-independent region of the material response in ET state is limited to $\epsilon = 0.3$. Furthermore, it can be observed that from the second cycle, the cyclic response is substantially stable, showing negligible variations of maximum stress and hysteresis area.

The stored (w_s/w_{tot}) and dissipated (w_d/w_{tot}) energy fractions are used to compare the energy density trends in the different states of deformation. The results, obtained from tests performed at $\dot{\epsilon} = 0.01\ s^{-1}$ for UT and PS, and from tests performed at $\dot{\epsilon} = 0.05\ s^{-1}$ for ET, are reported in Figure 18.

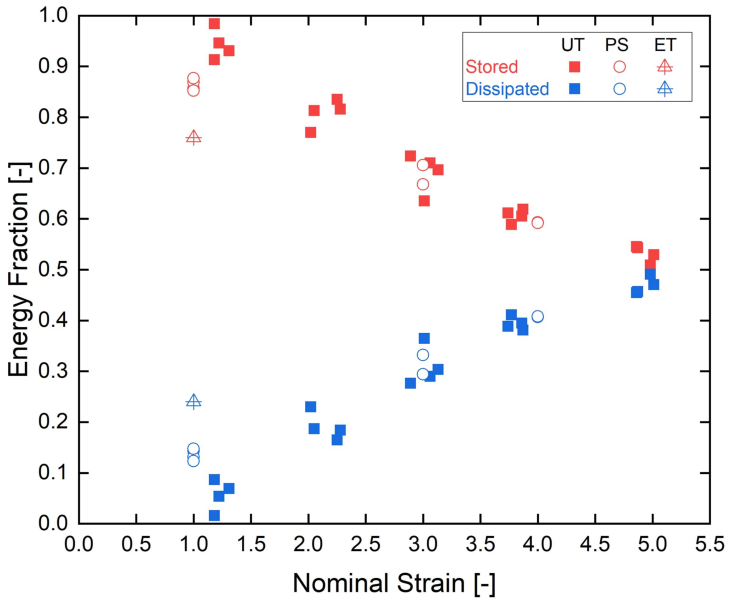

Figure 18: Stored (red) and dissipated (blue) energy fractions relevant to the first cycle for uniaxial tension (squares) and pure shear (circles) specimens subjected to cyclic tests at $\dot{\epsilon} = 0.01\ s^{-1}$, and equibiaxial tension (triangles) specimens subjected to cyclic tests at $\dot{\epsilon} = 0.05\ s^{-1}$. All tests performed at T = 23°C.

It can be seen that for both UT and PS states w_s/w_{tot} is close to 1 for $\epsilon \approx 1$, highlighting how negligible dissipation occurs below this strain level, although a slightly larger dissipated fraction is observed for the PS specimens, compared to the UT ones. The values of the energy fractions become comparable for the two deformation states for $3 \leq \epsilon \leq 4$ and, for UT, the two energy fractions become almost equal at $\epsilon \approx 5$. On the contrary, the value of dissipated energy fraction for the ET state at $\epsilon \approx 1$ is almost twice the PS value, highlighting how dissipation is not negligible at this strain level for this deformation state.

The knowledge of the dissipative behaviour of Ecoflex 00-50 and its dependence on both the strain rate and state of deformation considered are fundamental for the future constitutive modelling of the material, to be used to predict its response in more realistic applications, where it is subjected to complex loading states and histories.

4.3. Temperature effects

In Figure 19 the nominal stress-strain curves obtained from tensile tests performed on strip-shaped specimens at $\dot{\epsilon} = 0.1\ s^{-1}$ at different temperatures are reported. In order to compare the material behaviour at different temperatures, the highest and lowest experimental nominal stress-strain curves with variability intervals (the area between the two curves) for each testing temperature is reported.

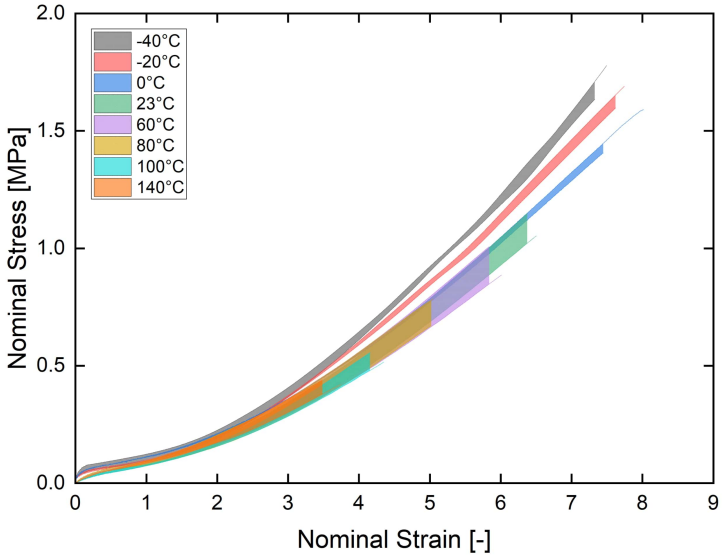

Figure 19: Ecoflex 00-50 nominal stress-strain curves obtained at different testing temperatures (from -40°C to 140°C). Tests performed on strip specimens at $\dot{\epsilon} = 0.1\ s^{-1}$.

The material response variability for temperatures higher than or equal to 23°C (which will be referred to as "high-temperature range") is larger than the variability at temperatures lower than 23°C (which will be referred to as "low-temperature range"). Generally speaking, given the curves dispersion, it can be stated that the variation in the material response in the strain range explored is not significant for tests performed in the high-temperature range. The main effect of increasing temperature in the high-temperature range is a progressive decrease in the material stress and strain at failure, with respect to their values at 23°C. On the contrary, in the low-temperature range, the material shows a higher stiffness at low strains and higher stress at high strains, especially at T=-20°C and at T=-40°C. In [28], it is highlighted

how, for unfilled silicone elastomers, the stiffness in the low-strain region increases as the temperature increases: this trend is not consistent with what has been observed in this work for Ecoflex 00-50, supporting the idea that the studied material contains a reinforcing filler as proposed in [6, 8]. In fact, the filler-related contribution to the material stiffness, associated with an enthalpy-related response, becomes more significant at low temperatures where the elastomer-related contribution, associated with an entropy-related response, decreases; the overall filler-elastomer system mobility is therefore reduced in the low-temperature range, resulting in a stiffer response upon stretching the material [29].

Overall, the effect of temperature on Ecoflex 00-50 response is complex and, to the best of the authors' knowledge, an accurate model able to reproduce such behaviour has not been proposed yet; on the other hand, the ultimate stress and strain show a clear dependence on temperature, which is presented and discussed following the concept of failure envelope [21, 22], introduced in order to determine a functional relation between ultimate stress (σ_U) and strain (ϵ_U), independent of testing method and conditions: by reporting the ultimate stress versus the ultimate strain on a double logarithmic plot, the curve interpolating the rupture points, obtained in different testing conditions, identifies the failure envelope which is unique for any material and is independent of time and temperature. The ultimate stress values are multiplied by a temperature factor T_0/T in order to reduce all values to the arbitrary reference temperature T_0 (chosen to be 296 K), although no direct experimental evidence was presented to justify the procedure for ultimate stress superposition in [21]. The Ecoflex 00-50 rupture points relevant to the tests performed at different temperatures are reported in Figure 20 in a log-log scale plot.

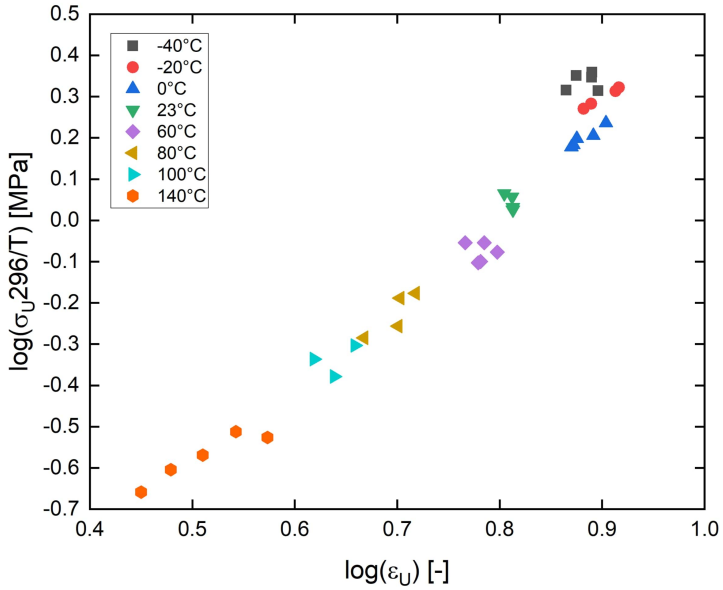

Figure 20: Relationship between ultimate stress (normalized by a temperature factor T_0/T) and ultimate strain on a double logarithmic plot. Ultimate tensile data obtained from tests performed on strip specimens at different temperatures (from -40°C to 140°C) and $\dot{\epsilon} = 0.1\ s^{-1}$.

Some scattering of experimental data exists, especially for the values obtained at 140°C. However, it is evident how the points clearly define a curve, which identifies the failure envelope of Ecoflex 00-50, resembling the ones reported in [21] for other unfilled elastomers. Two separate regimes can be identified in the curve: the high-temperature region (corresponding to $T \geq 23$°C), where a linear trend of the envelope is observed with increasing temperature, and a low-temperature regime (corresponding to $T < 23$°C) where a change of trend is observed, since ϵ_U remains almost constant, whereas σ_U slightly increases with decreasing temperature.

An alternative representation of stress and strain at failure is reported in [21]. From the values of stress and strain, it is possible to define a linear relationship between the two, according to Martin, Roth and Stiehler (MRS) equation [30]:

$$\sigma = E_e \left(\frac{\lambda - 1}{\lambda^2} \right) exp \left[A \left(\lambda - \frac{1}{\lambda} \right) \right] \tag{11}$$

where E_e is the equilibrium tensile modulus of the material, and A is an empirical constant. This relationship can be applied to high-temperature ultimate stress and strain values since the stress-strain curves obtained from tests in the high-temperature range correspond to the equilibrium response of the material, showing a trend not dependent on testing temperature [22]. The same multiplying factor used in the failure envelope representation is employed to reduce data obtained at different temperatures to a single reference temperature. Thus, the logarithmic form for ultimate tensile data of Equation (11) becomes:

$$log\left[\frac{\sigma_U \lambda_U^2}{(\lambda_U - 1)}\frac{296}{T}\right] = log\left(E_e \frac{296}{T}\right) + 2.303A\left(\lambda_U - \frac{1}{\lambda_U}\right) \qquad (12)$$

which, in double logarithmic plane, corresponds to a linear relation with slope $2.303A$ and intercept $log\,(E_e 296/T)$, as shown in Figure 21.

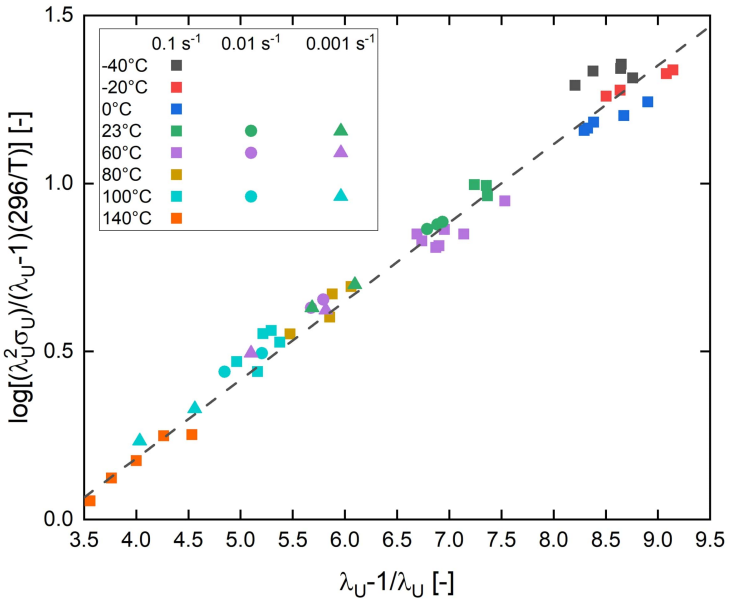

Figure 21: Martin, Roth and Stiehler (MRS) representation of ultimate tensile data, obtained at different temperatures (from -40°C to 140°C) and strain rates (from $\dot{\epsilon} = 0.001\ s^{-1}$ to $\dot{\epsilon} = 0.1\ s^{-1}$), and theoretical linear trend (see Equation (12), dashed line).

It can be seen that the ultimate data obtained in the temperature range between 23°C and 140°C fall perfectly on the theoretical line, whereas the data measured in the low-temperature range (below 23°C) show, as expected,

a very limited degree of deviation from the predicted behaviour. This is in agreement with the results reported in [22] for various unfilled elastomers, where it is observed that only the high-temperature ultimate stress and strain identify the equilibrium behaviour of the material and low-temperature data do not fall on the linear trend. Furthermore, from the slope of the linear trend, it is found that $A = 0.1$ MPa and from the intercept $E_e = 0.17$ MPa (at 23°C), which is the same value as the one estimated from the slope of the linear region of the stress-strain curves (up to $\epsilon = 0.1$), as reported in Table 2.

T, [°C]	$E(\epsilon = 0.1)$**, [MPa]**	ϵ_U**, [-]**	σ_U**, [MPa]**
23	0.17 ± 0.02	6.46 ± 0.06	1.10 ± 0.05

Table 2: Averaged values (with relevant standard deviation) of tensile modulus, ultimate strain and ultimate stress obtained from tests performed at T = 23°C and $\dot{\epsilon} = 0.1\ s^{-1}$.

Comparing the results reported in Table 1, obtained during tensile tests performed at $\dot{\epsilon} = 0.1\ s^{-1}$, and those reported in Table 2, performed at the same strain rate on strip specimens, it is noticeable how, as expected, the tensile modulus corresponding to strip specimens is twice the modulus of dumbbell specimens: this is a result of the adopted specimen geometry which increases the apparent modulus of the material at low strain levels. On the other hand, the values of ultimate stress and strain obtained with the two specimen geometries are comparable (also considering the large variability observed for dumbbell specimens): this can be attributed to the deformation state experienced by the specimen during tensile testing, which becomes more and more similar to UT as strain increases. Therefore, the last considerations about ultimate stress and strain can be applied to the UT deformation state.

To evaluate the predictive capability of the obtained MRS equation, tests at 23°C, 60°C and 120°C were repeated at different strain rates: as can be observed in Figure 21, the obtained data lie on the same curve, indicating that the method here adopted can be used to predict ultimate stresses and strains of Ecoflex 00-50 in a wide range of temperatures and strain rates.

5. Conclusions

In this work, the mechanical behaviour of Ecoflex Shore hardness 00-50 has been characterized in different deformation states, namely uniaxial tension,

pure shear and equibiaxial tension; the effects of strain rate and temperature on the mechanical response were investigated. The main findings are summarized as follows:

- The material response for strain levels between 0 and 2 in uniaxial tension and pure shear and between 0 and 0.3 in equibiaxial tension is practically unaffected by the strain rate. In cyclic tests, for applied strain values up to 2, the material showed negligible energy dissipation when tested under uniaxial tension and in pure shear loading conditions. In contrast, non-negligible energy dissipation occurred in equibiaxial tension.

- The overall stress-strain trend is not affected by the temperature in the temperature range above 23°C. However, a decrease in ultimate material properties with increasing temperature was observed. For temperatures below room temperature, an increase in stiffness in the low-strain region was observed, as well as an increase in stress in the high-strain region.

- The failure envelope can be used to represent Ecoflex 00-50 ultimate tensile data at different temperatures, and the Martin-Roth-Stiehler (MRS) equation constitutes a valuable engineering tool, allowing an adequate description of the combined effects of strain rate and temperature on the stress and strain at failure of the material.

This extensive thermo-mechanical characterization highlighted the need to consider many different aspects, which often influence each other, to be able to, in the future, correctly model and predict the material response in realistic loading scenarios.

Declaration of competing interest

The authors declare that they have no known competing financial interests or personal relationships that could have appeared to influence the work reported in this paper.

References

[1] S. J. Clarson, Silicones and silicone-modified materials: A concise overview, ACS Symposium Series (2003) 1–10doi:https://doi.org/10.1021/bk-2003-0838.ch001.

[2] A. M. Stricher, R. G. Rinaldi, C. Barrès, F. Ganachaud, L. Chazeau, How i met your elastomers: from network topology to mechanical behaviours of conventional silicone materials, RSC Advances 5 (66) (2015) 53713–53725. doi:https://doi.org/10.1039/C5RA06965C.

[3] Z. Liao, M. Hossain, X. Yao, R. Navaratne, G. Chagnon, A comprehensive thermo-viscoelastic experimental investigation of ecoflex polymer, Polymer Testing 86 (2020) 106478. doi:https://doi.org/10.1016/j.polymertesting.2020.106478.

[4] L. Bernardi, R. Hopf, A. Ferrari, A. E. Ehret, E. Mazza, On the large strain deformation behavior of silicone-based elastomers for biomedical applications, Polymer Testing 58 (2017) 189–198. doi:http://dx.doi.org/10.1016/j.polymertesting.2016.12.029.

[5] Z. Liao, M. Hossain, An additively manufactured silicone polymer: Thermo-viscoelastic experimental study and computational modelling, Additive Manufacturing 35 (2020) 101395. doi:https://doi.org/10.1016/j.addma.2020.101395.

[6] E. Luis, H. M. Pan, A. K. Bastola, R. Bajpai, S. L. Sing, J. Song, W. Y. Yeong, 3d printed silicone meniscus implants: Influence of the 3d printing process on properties of silicone implants, Polymers 12 (2020) 2136. doi:https://doi.org/10.3390/polym12092136.

[7] R. Hopf, L. Bernardi, J. Menze, M. Zündel, E. Mazza, A. E. Ehret, Experimental and theoretical analyses of the age-dependent large-strain behavior of sylgard 184 (10:1) silicone elastomer, Journal of the Mechanical Behavior of Biomedical Materials 60 (2016) 425–437. doi:http://dx.doi.org/10.1016/j.jmbbm.2016.02.022.

[8] S. Krpovic, K. Dam-Johansen, A. L. Skov, Importance of mullins effect in commercial silicone elastomer formulations for soft robotics, Journal of Applied Polymer Science 138 (19) (2020) 50380. doi:https://doi.org/10.1002/app.50380.

[9] M. Amjadi, Y. J. Yoon, I. Park, Ultra-stretchable and skin-mountable strain sensors using carbon nanotubes–ecoflex nanocomposites, Nanotechnology 26 (2015) 375501. doi:https://doi.org/10.1088/0957-4484/26/37/375501.

[10] Y. Jiang, Y. Wang, Y. K. Mishra, R. Adelung, Y. Yang, Stretchable cnts-ecoflex composite as variable-transmittance skin for ultrasensitive strain sensing, Advanced Materials Technologies 3 (2018) 1800248. doi:https://doi.org/10.1002/admt.201800248.

[11] H. Yuk, T. Zhang, G. A. Parada, X. Liu, X. Zhao, Skin-inspired hydrogel–elastomer hybrids with robust interfaces and functional microstructures, Nature Communications 7 (1) (Jun 2016). doi:10.1038/ncomms12028.

[12] S. H. Kim, S. Jung, I. S. Yoon, C. Lee, Y. Oh, J.-M. Hong, Ultrastretchable conductor fabricated on skin-like hydrogel–elastomer hybrid substrates for skin electronics, Advanced Materials 30 (26) (2018) 1800109. doi:https://doi.org/10.1002/adma.201800109.

[13] R. V. Martinez, C. R. Fish, X. Chen, G. M. Whitesides, Elastomeric origami: Programmable paper-elastomer composites as pneumatic actuators, Advanced Functional Materials 22 (7) (2012) 1376–1384. doi:https://doi.org/10.1002/adfm.201102978.

[14] J. L. Sparks, N. A. Vavalle, B. Kasting, K. E. Long, M. L. Tanaka, P. A. Sanger, K. Schnell, T. A. Conner-Kerr, Use of silicone materials to simulate tissue biomechanics as related to deep tissue injury, Advances in Skin & Wound Care 28 (2015) 59–68. doi:https://doi.org/10.1097/01.asw.0000460127.47415.6e.

[15] J. Yu, X. Hou, M. Cui, N. Zhang, S. Zhang, J. He, X. Chou, Skin-conformal batio3/ecoflex-based piezoelectric nanogenerator for self-powered human motion monitoring, Materials Letters 269 (2020) 127686. doi:https://doi.org/10.1016/j.matlet.2020.127686.

[16] H. Mai, R. Mutlu, C. Tawk, G. Alici, V. Sencadas, Ultra-stretchable mwcnt–ecoflex piezoresistive sensors for human motion detection applications, Composites Science and Technology 173 (2019) 118–124. doi:https://doi.org/10.1016/j.compscitech.2019.02.001.

[17] Z. Wen, J. Yang, H. Ding, W. Zhang, D. Wu, J. Xu, Z. Shi, T. Xu, Y. Tian, X. Li, Ultra-highly sensitive, low hysteretic and flexible pressure sensor based on porous mwcnts/ecoflex elastomer composites, Journal of Materials Science: Materials in Electronics 29 (24) (2018) 20978–20983. doi:10.1007/s10854-018-0242-3.

[18] L. Mullins, Softening of rubber by deformation, Rubber Chemistry and Technology 42 (1) (1969) 339–362. doi:https://doi.org/10.5254/1.3539210.

[19] Z. Liao, M. Hossain, Y. Xiaohu, Ecoflex polymer of different shore hardnesses: Experimental investigations and constitutive modelling, Mechanics of Materials 144 (2019) 103366. doi:https://doi.org/10.1016/j.mechmat.2020.103366.

[20] Z. Liao, J. Yang, M. Hossain, G. Chagnon, L. Jing, Y. Xiaohu, On the stress recovery behaviour of ecoflex silicone rubbers, International Journal of Mechanical Sciences 206 (2021) 106624. doi:https://doi.org/10.1016/j.ijmecsci.2021.106624.

[21] T. L. Smith, Ultimate tensile properties of elastomers. i. characterization by a time and temperature independent failure envelope, Polymer Science Part A: General Papers 1 (12) (1963) 3597–3615. doi:https://doi.org/10.1002/pol.1963.100011207.

[22] T. L. Smith, Ultimate tensile properties of elastomers. ii. comparison of failure envelopes for unfilled vulcanizates, Journal of Applied Physics 35 (1) (1964) 27–36. doi:https://doi.org/10.1063/1.1713094.

[23] J. C. Halpin, Fracture of amorphous polymeric solids: Time to break, Journal of Applied Physics 35 (11) (1964) 3133–3141. doi:https://doi.org/10.1063/1.1713191.

[24] F. Beuche, J. C. Halpin, Molecular strength of the tensile strength of gum elastomers, Journal of Applied Physics 35 (1) (1964) 36–41. doi:https://doi.org/10.1063/1.1713095.

[25] F. Caimmi, R. Calabrò, F. Briatico-Vangosa, C. Marano, M. Rink, Toughness of natural rubber compounds under biaxial loading, Engineering Fracture Mechanics 149 (2015) 250–261. doi:https://doi.org/10.1016/j.engfracmech.2015.08.003.

[26] L. R. G. Treloar, The Physics of Rubber Elasticity, 3rd ed., Oxford University Press, Oxford, 2009.

[27] L. R. G. Treloar, The elasticity of a network of long-chain molecules—ii, Transactions of the Faraday Society 39 (1943) 241–246. doi:https://doi.org/10.1039/tf9433900241.

[28] T. Rey, G. Chagnon, J. B. Le Cam, B. Favier, Influence of the temperature on the mechanical behaviour of filled and unfilled silicone rubbers, Polymer Testing 32 (3) (2013) 492–501. doi:https://doi.org/10.1016/j.polymertesting.2013.01.008.

[29] X. Li, T. Bai, Z. Li, L. Liu, Influence of the temperature on the hyperelastic mechanical behavior of carbon black filled natural rubbers, Mechanics of Materials 95 (2016) 136–145. doi:https://doi.org/10.1016/j.mechmat.2016.01.010.

[30] G. M. Martin, F. L. Roth, R. D. Stiehler, Behavior of pure-gum rubber vulcanizates in tension, Rubber Chemistry and Technology 30 (3) (1957) 876–888. doi:https://doi.org/10.5254/1.3542733.